Validity of the catenary model for moving submarine cables with negative buoyancy

Juliette Drupt[1], Claire Dune[1], Andrew I. Comport[2], Vincent Hugel[1]

***Abstract*— In the field of underwater robotics, tethers are the dominant method used to provide real time communication with underwater vehicles. Estimating their shape is a key element in preventing entanglements and limiting their mechanical effects on the vehicles. In addition, the tether shape constrains the pose of the vehicle at its attachment point, and could thus be used for vehicle localization purposes given an accurate tether model. This work focuses on a simple model of flexible non-rigid hanging cables, namely the catenary model, and presents an experimental evaluation of the validity of this model to approximate the shape of dynamically moving underwater tethers with negative buoyancy using motion tracking.**

I. Introduction

Underwater communications suffer from the absorption of electromagnetic waves within only a few centimeters of water. The mainstream way to provide real time communication between an underwater robot and a surface vessel is then to connect them through a physical link, or tether. Such remotely operated vehicles (ROVs) allow to achieve tasks that cannot be fully automated and require precision and adaptability. The tether can also provide energy to the ROV for better autonomy with a lighter embedded payload.

The design of the tether and of its buoyancy depends on the intended application. Thus, a tether with positive or neutral buoyancy will avoid lifting sediments or getting stuck in reliefs by dragging along the seabed if the robot operates close to it. On the other hand, cables with negative buoyancy are required to transport a significant amount of energy to working ROVs over distances of several hundred meters.

The tether affects the ROV's mobility. First, the mechanical action of the tether limits the ROV's motion and involves increased energy consumption. Second, the risk of tether entanglement restricts operation in cluttered environments. These effects can be limited by tether management strategies [1] which can be passive [2], [3] or active [4], [5]. When active, knowledge of the system's state is necessary, hence there is an interest in the estimation of the tether shape. Furthermore, knowing the tether's 3D shape can enable locating the ROV at its attachment point.

Some underwater cables are designed as proprioceptive sensors in order to measure their own shape. Optical-fiber cables measure their deformations using reflectometry techniques [6], [7]. Such cables can be used to locate connected underwater vessels [8]. Another version of optical fiber cable shape sensing consists in adding an external optical fiber sensor coating on a cable [9]. Such cables are, however, fragile and extremely expensive. The cable's shape can also be estimated from the measurements of inertial sensors placed along it [10]. However, these methods need to use a specifically built tether. Other strategies rely on physical or geometrical cable models. A physical model can be derived from the hydrodynamics of the cable and the forces that apply to it [11], [12], [13], [14]. Such models are the most complete and physically accurate, but they are computationally expensive and require the knowledge of many parameters which cannot be measured easily in real conditions, such as water current or parameters of the thrusters. Simpler models are then commonly preferred. The cable can be artificially constrained to a simplified geometric shape, for example by constraining the cable to be piecewise linear by adding weights or sliding floaters [2], [3]. Other works use the catenary model for underwater applications [5], [15], or aerial applications [16], [17], [18]. The catenary model is defined as the shape of an idealized homogeneous hanging cable with fixed length and fixed ends, only subject to its own weight in air. Underwater cables are also submitted to a buoyancy force, opposed to the weight. The catenary model then only applies to cables for which the resulting vertical force is non-zero, i.e. only positively and negatively buoyant cables. This model is particularly interesting because of its simplicity, but extending it to an underwater cable with moving ends assumes that the hydrodynamic forces exerced on the cable are negligible compared to its weight, and that the motion is such that the cable is always close to its state.

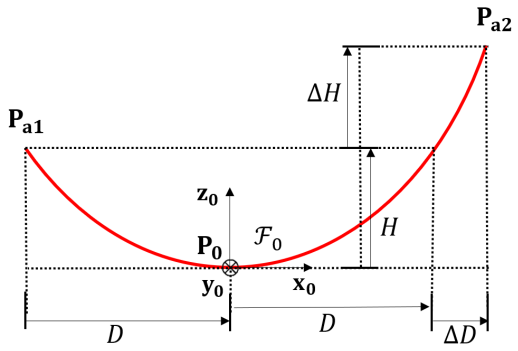

Fig. 1: Catenary shape parameterization.

This paper presents an experimental study in order to evaluate whether the catenary model may be use to model a weighing underwater cable with moving ends, in the absence of currents. This study is based on tracking the motion of two negatively buoyant cables of different linear mass in a

[1]COSMER Laboratory EA7398, Université de Toulon, France
[2]CNRS I3S Laboratory, Université Côte d'Azur, Sophia Antipolis, France

pool. Their shape is then compard to the closest catenary curve. This comparison is based on three properties of the catenary model for static hanging cables:

- the cable should lie in a plane
- this plane should be vertical with respect to gravity
- the 2D shape of the cable in this plane should fit a catenary 2D curve.

Section II defines the catenary model and gives its equations in 2D and 3D. Section III presents the numerical shape estimation method and the measurements used to validate the model. The experimental results are presented and discussed in Section IV. Finally, Section V concludes on this study.

II. Catenary equations for cable modeling

A. Static hanging cable

Let us consider an homogeneous hanging cable with fixed length and fixed ends, only subject to its own weight. It can be shown that it conforms to a catenary shape defined in a vertical plane [19].

Let $\mathcal{F}_{2D}$ be an orthonormal 2D frame. The catenary curve is defined in $\mathcal{F}_{2D}$ by:

$$\forall x \in \mathbb{R}, y = \frac{1}{C}[\cosh(Cx) - 1] \tag{1}$$

where $C \in \mathbb{R}^*$ and (x, y) denote the coordinates of a 2D point in $\mathcal{F}_{2D}$.

Figure 1 shows the parameterization of a catenary shape for a cable with fixed length L whose attachment points are $\mathbf{P}_{a1}$ and $\mathbf{P}_{a2}$. Let us define a direct Cartesian frame $\mathcal{F}_0$ for the catenary, such that its center is $\mathbf{P}_0$, the lowest point of the catenary, $\mathbf{z}_0$ is vertical, and $\mathbf{y}_0$ is orthogonal to the vertical plane that contains $\mathbf{P}_{a1}$ and $\mathbf{P}_{a2}$. The coordinates (X, Y, Z) of the cable points expressed in frame $\mathcal{F}_0$ are:

$$\forall X \in [-D, D + \Delta D], \begin{cases} Y = 0 \\ Z = \frac{1}{C}[\cosh(CX) - 1] \end{cases} \tag{2}$$

C can be expressed geometrically as a fonction of parameters the cable's sag H, the difference of elevation of the attachment points ΔH and the cable length L. H and ΔH are shown in Figure 1.

$$C = \frac{2(2H + \Delta H + 2L\sqrt{H\frac{H+\Delta H}{L^2-\Delta H^2}})}{L^2 - (2H + \Delta H)^2} \tag{3}$$

C can also be defined from the laws of physics as:

$$C = \frac{\mu g}{T_0} \tag{4}$$

where μ is the cable's linear mass, g is the value of gravity on Earth and T_0 is the tension at $\mathbf{P}_0$.

It can be shown that this model extends to an homogeneous hanging cable with fixed length and fixed ends in a fluid, only subject to its own weight and to Archimedes' buoyancy with a non zero resulting force, with:

$$C = \frac{(\mu - v_l\rho)g}{T_0} \tag{5}$$

where v_l and ρ denote respectively the cable's linear volume and the fluid's density.

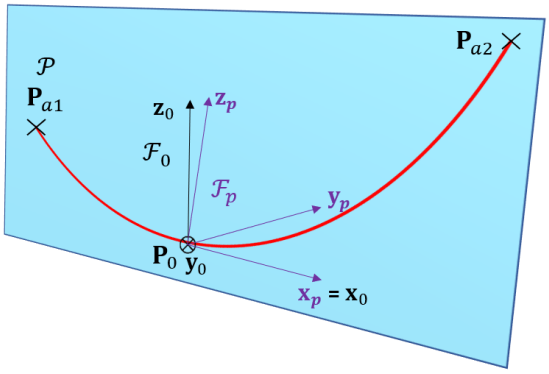

Fig. 2: Inclined catenary model

B. Inclined hanging cable in water

As soon as the cable is moved in the water, it may happen that the current or the movement of the ends leads the cable to a transitional position in an inclined plane. In this paper, the cable shape in this plane will be studied to determine if its deviation from the catenary model is significant. Let this situation be called the inclined catenary.

Now let the inclined catenary curve model be defined as a 3-dimensional catenary included in a non-vertical plane $\mathcal{P}$, as represented in Figure 2. $\mathcal{F}_w$ is a world frame with origin P_w and $\mathbf{z}_w$ vertical and pointing upwards. Frame $\mathcal{F}_0$ is defined as previously, such that its center is $\mathbf{P}_0$, the lowest point of the catenary, $\mathbf{z}_0$ is vertical upwards, and $\mathbf{y}_0$ is orthogonal to the vertical plane that contains $\mathbf{P}_{a1}$ and $\mathbf{P}_{a2}$. The transformation from $\mathcal{F}_0$ to $\mathcal{F}_w$ is then:

$${}^w\mathbf{T}_0 = \begin{bmatrix} \mathbf{R}_z(\psi) & {}^w\mathbf{P_0} \\ \mathbf{0_{1\times3}} & 1 \end{bmatrix} \tag{6}$$

where $\mathbf{R}_z(\psi)$ denotes a yaw rotation of angle ψ and ${}^w\mathbf{P}_0$ is the coordinate vector of $\mathbf{P}_0$ in $\mathcal{F}_w$.

Let define $\mathcal{F}_p$ be defined with origin $\mathbf{P}_0$, such that $\mathbf{x}_p = \mathbf{x}_0$ and $\mathbf{z}_p$ is the normalized projection of $\mathbf{z}_0$ in plane $\mathcal{P}$. $\mathbf{y}_p$ is then normal to $\mathcal{P}$. The transformation between frames $\mathcal{F}_p$ and $\mathcal{F}_0$ is then a pure rotation of angle α around $\mathbf{x}_0$:

$${}^0\mathbf{T}_p = \begin{bmatrix} \mathbf{R}_x(\alpha) & \mathbf{0_{3\times1}} \\ \mathbf{0_{1\times3}} & 1 \end{bmatrix} \tag{7}$$

The coordinates of the inclined catenary curve contained in plane $\mathcal{P}$ are given in frame $\mathcal{F}_p$ by $({}^pX, {}^pY, {}^pZ)$ where:

$$\begin{cases} {}^pY = 0 \\ {}^pZ = \frac{1}{C}[\cosh(C\,{}^pX) - 1] \end{cases} \tag{8}$$

In frame $\mathcal{F}_w$, the coordinate vector of a point $\mathbf{P}$ belonging to the inclined catenary curve is finally ${}^w\mathbf{P} = {}^w\mathbf{T}_0\,{}^0\mathbf{T}_p\,{}^p\mathbf{P}$. Alternatively, an inclined catenary curve is fully defined by the set of parameters $(\mathcal{P}, C, {}^wX_0, {}^wZ_0)$ where ${}^wX_0$ and ${}^wZ_0$ denote the $\mathbf{x}$ and $\mathbf{y}$ coordinates of $\mathbf{P}_0$ in $\mathcal{F}_w$. ${}^wY_0$ can be computed from ${}^wX_0$ and ${}^wZ_0$ based on the constraint $\mathbf{P}_0 \in \mathcal{P}$.

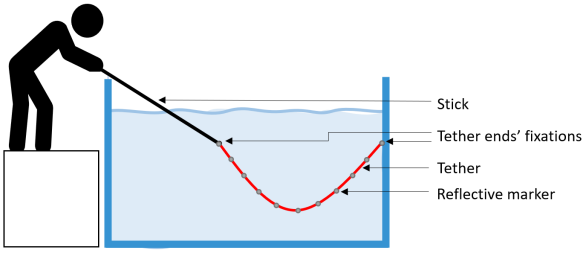

Fig. 3: Experimental setup scheme.

III. Numerical estimation method and evaluation metrics

A. Catenary curve fitting

Let a set of N 3D points that belong to a cable be defined as $\{\mathbf{P}_i\}_{i\in\{1...N\}}$. The plane $\mathcal{P}$ is defined as the plane that best contains the points $\{\mathbf{P}_i\}_{i\in\{1...N\}}$. It is computed by minimizing point-plane distance. We use `fminsearch` Matlab function which implements the Nelder-Mead simplex algorithm as described in [20]. An initial guess is computed using three arbitrarily choosen tracked points.

In a second time, the points $\{\mathbf{P}_i\}_{i\in\{1...N\}}$ are projected on $\mathcal{P}$. The inclined catenary curve that best fits the resulting points in plane $\mathcal{P}$ is then estimated. An initial guess is computed by calculating the vertical catenary curve between the pair of visible tracked points that are the closest to the cable's ends. Again, the optimization uses `fminsearch` Matlab function.

B. Catenary shape measurements

Three indicators have been selected to characterize the catenary shape of the cable:

- the root mean square error (RMSE) $e_{\mathcal{P}}$ of the distance between the tracked points and plane $\mathcal{P}$.
- inclination of the plane $\mathcal{P}$ with respect to the vertical, *i.e.* the absolute value α of the angle between the normal to the plane $\mathcal{P}$ and the normal to the vertical plane with the same yaw orientation as plane $\mathcal{P}$ in $\mathcal{F}_w$.
- the RMSE $e_{\mathcal{C}}$ of the distance between the projection of points $\{\mathbf{P}_i\}_{i\in\{1...N\}}$ in plane $\mathcal{P}$ and the points with same x-coordinate in frame $\mathcal{F}_p$ that belong to the fitted inclined catenary curve.

IV. Experimental Results

Figure 3 represents the experimental setup. A cable is deployed in a pool, with one end tied to a fixed point and the other end tied to a stick. The stick is then moved by an operator. The cable is equipped with regularly spaced reflective markers that are tracked by a motion capture system (see Figure 3). This experiment is reproduced with two cables of different linear mass μ, diameter Φ, and material: a metal chain and a thin rope, denoted respectively Cable 1 and Cable 2. Table I gives their respective characteristics. $\widehat{L}$ is the approximate cable length.

The experiments are conducted in a pool, in plain water, at shallow depth (<4m).

TABLE I: Characteristics of the cables. Since Cable 1 is a chain, the given diameter d corresponds to the width of a link.

	Cable 1	Cable 2
μ when wet (kg/m)	$9.20 \times 10^{-}2$	$2.26 \times 10^{-}2$
$\widehat{L}$ (mm)	3500	2000
Φ (mm)	10	5
Material	Steel	Fabric
Max number of tracked points	12	9
Spacing between markers (mm)	245	200

A 166.98s tracking sequence was recorded for Cable 1, as well as a 252.68s long sequence for Cable 2. Figures 4 to 7 illustrate the typical behavior of the cables during subsequences that include movements of the tether's end point in various directions with slow and rapid motion, and correspond to time periods when the cable was well tracked by the motion capture system.

Figures 4 and 6 show the computed values of α, $e_{\mathcal{P}}$, $e_{\mathcal{C}}$ and catenary parameter C for Cables 1 and 2 respectively. Figures 5 and 7 show the number N of tracked points and which tracked points are visible, as well as the velocity and acceleration of the mobile end of the cable in $\mathcal{F}_w$ and the distance d between the cable's ends during the same subsequence as Figures 4 and 6, for Cable 1 and Cable 2 respectively.

One can observe that the greater the distance d, the smaller the parameter C. Indeed, an increased distance between the end points implies more tension in the cable and thus a lower C according to equations (4) and (5). The peaks in the curves of α, $e_{\mathcal{P}}$ and $e_{\mathcal{C}}$ occur when only few points are visible or when the set of visible tracked points changes. The set of visible points changes when the tracking system stops to detect some points or detects new ones. The more visible tracked points the more reliable the catenary likelihood indicators.

Table II gives the mean, minimum, maximum, median and standard deviation σ of indicators α, $e_{\mathcal{P}}$ and $e_{\mathcal{C}}$ for Cable 1's full tracking sequence. The same results for Cable 2's full sequence are displayed in Table III. Only the values computed when $N > 6$ are considered reliable and included in these statistics.

TABLE II: Results for Cable 1

	α (°)	$e_{\mathcal{P}}$ (mm)	$e_{\mathcal{C}}$ (mm)
mean	2.67	0.60	12.6
min	2.94×10^{-5}	0.08	0.19
max	29.1	4.55	286
median	1.70	0.45	4.38
σ	3.08	0.42	27.67

On the one hand, the results in Table II show that Cable 1's shape stays very close to the catenary shape along the entire

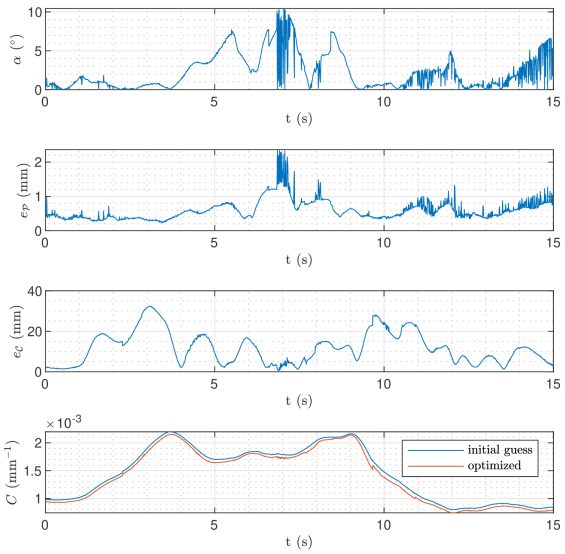

Fig. 4: Variations of α, $e_{\mathcal{P}}$, $e_{\mathcal{C}}$ and catenary parameter C during a part of the whole Cable 1 tracking sequence: 15s from $t = 0s$ from the full record.

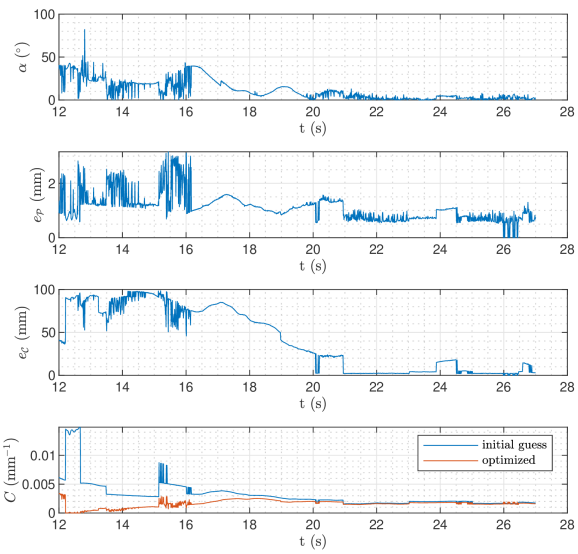

Fig. 6: Variations of α, $e_{\mathcal{P}}$, $e_{\mathcal{C}}$ and catenary parameter C during a part of the whole Cable 2 tracking sequence: 15s from $t = 12s$ from the full record.

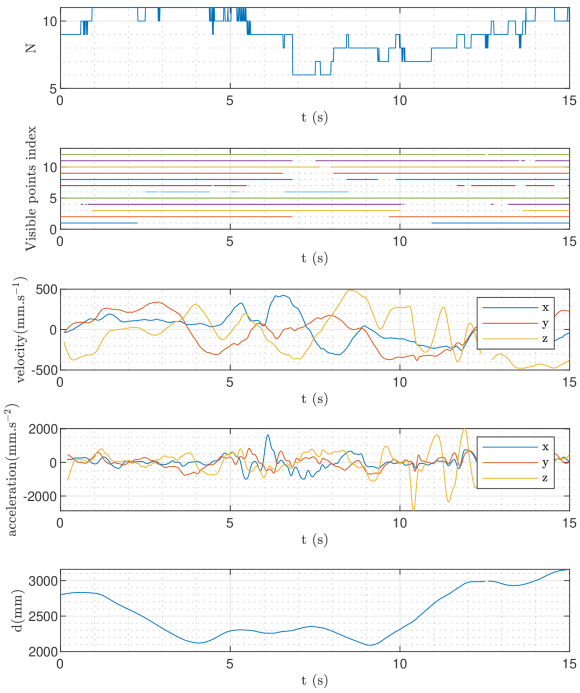

Fig. 5: Variations of the number of tracked points N, tracked points visibility, end point velocity and acceleration in $\mathcal{F}_w$ and distance between the cable's ends during a part of the whole Cable 1 tracking sequence: 15s from $t = 0s$ from the full record. The tracked point on the mobile end has index 12.

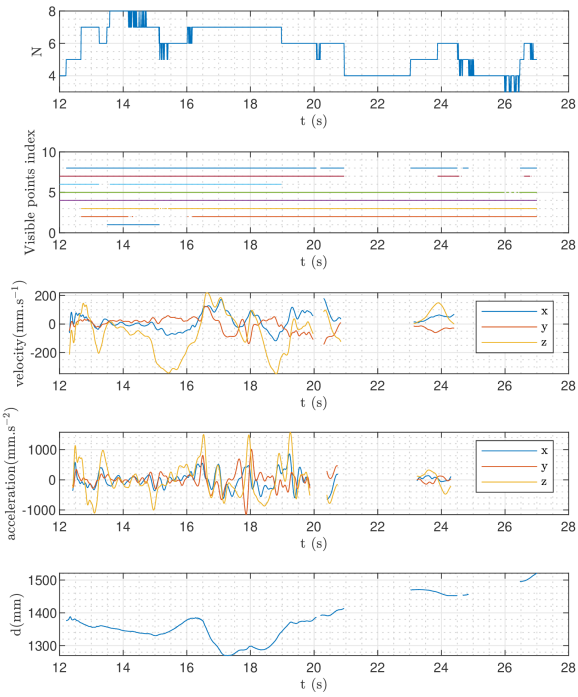

Fig. 7: Variations of the number of tracked points N, tracked points visibility, end point velocity and acceleration in $\mathcal{F}_w$ and distance between the cable's ends during a part of the whole Cable 2 tracking sequence: 15s from $t = 12s$ from the full record. The tracked point on the mobile end has index 8.

TABLE III: Results for Cable 2

	α (°)	$e_{\mathcal{P}}$ (mm)	$e_{\mathcal{C}}$ (mm)
mean	16.52	1.14	52.2
min	6.81×10^{-4}	0.10	0.30
max	82.0	3.65	500
median	11.3	1.09	19.2
σ	15.1	0.46	69.1

sequence. The mean, median and standard deviation of $e_{\mathcal{P}}$ are very small with respect to the cable length, with an order of magnitude of 5×10^{-4} m (cable length of approximately 3.5m). This validates the assumption of a planar cable. The mean, median and standard deviation of angle α are also small, with an order of magnitude of $1°$, showing that this plane can be well approximated as vertical. The maximum value for α in the whole sequence is about $30°$, but the small standard variation of about $3°$ indicates that such an important angle is rare. This extremum corresponds to a fast lateral movement of the cable. Finally, $e_{\mathcal{C}}$ and their variations are small on the scale of Cable 1's length, with less than 1% of its length, indicating that it can be well approximated by a catenary shape in the cable plane. Even the maximal value of e_C represents only approximately 10% of Cable 1's length. Cable 1 can then be well approximated by the catenary model introduced in Section II, even with its endpoints moving. In addition, the small maximal values and standard deviation of e_P and e_C show that even if the cable's plane may be inclined from the vertical, it can then be well approximated by an inclined catenary curve as introduced in Section II-B.

On the other hand, the results in Table III show that the catenary model as defined in Section II is less accurate for Cable 2. $e_{\mathcal{P}}$ and its variations have the same order of magnitude than those of Cable 1. This indicates that the cable can be considered planar most of the time, but the mean value and variations of α show that this plane cannot be considered vertical in the general case. The maximum value of α shows that the cable's plane even came close to the horizontal plane at some point in the sequence. The mean, median and standard deviation of $e_{\mathcal{C}}$ are about four times higher than those of Cable 2, showing that even in the cable's plane, Cable 2 is much further from the catenary model than Cable 1. Qualitatively, the changes in direction of Cable 2's end point movements create inflection points on the cable, making its shape more different from a catenary at these moments. This does not occur with Cable 1 during the tracking sequence. One can notice that the mean, median and standard deviation of $e_{\mathcal{C}}$ are however still small with respect to the cable length. This shows that even a light cable like Cable 2 can be modelled by an inclined catenary curve as a first estimate. Such an approximation is nevertheless less accurate than modeling Cable 1 as a catenary.

Finally, these results show that the catenary curve is a good approximation of an underwater cable with moving endpoints if it has a "heavy enough" linear mass. Cables with lower linear mass may be better approximated by an inclined catenary by assuming that the cable's plane may be inclined an angle α from the vertical, but with lower accuracy. It is then a question of design to guarantee that the cable conforms to a catenary curve in a vertical plane. It must also be a compromise with keeping the cable light enough not to impede the robot's motion. In addition, it is necessary to take into account the water flow generated by the thrusters which can move the part of the cable located in their vicinity. The cable should thus be placed out of the thruster's flow as much as possible. Avoiding movements with abrupt changes of direction will also help to keep the model valid.

V. Conclusion and future work

In this work, two underwater cables with different linear mass were tracked using a motion capture system while moving one of their endpoints. The tracking data was then used to estimate the plane that best contained the cable, and the catenary shape that was the closest to the projection of the cable in this plane. Different metrics were used to characterize the catenary likelihood of the two cables. The results showed that the catenary equation still gives a good shape approximation for underwater cables having a large enough linear mass, even with their endpoints moving dynamically. Thus, the selection of such a cable when designing an underwater tethered system can simplify the cable's shape estimation by modelling it by a catenary curve, while maintaining a good accuracy.

The choice of the cable has to be a compromise between a cable heavy enough to conform into a catenary and light enough not to impede the robot's motion. Avoiding abrubt changes of direction in the ROV's motion will also contribute in keeping the catenary model valid. The length of the cable may also impact the validity of the model.

Finally, since the catenary model describes well a moving submarine cable with negative bouyancy under these design assumptions, this model may be used for a model-based cable shape estimation, which is planned for future works.

VI. Acknowledgment

This work is funded by the French Research Ministry, the CARTT of the IUT of Toulon. We would like to thank the CEPHISMER of the French Navy for their logistical support.

References

[1] R. Christ, *The ROV manual*, 2nd ed. Oxford, England: Butterworth-Heinemann, Dec. 2013.

[2] C. Viel, "Self-management of the umbilical of a rov for underwater exploration," *Ocean Engineering*, vol. 248, p. 110695, Mar. 2022.

[3] ——, "Self-management of ROV umbilical using sliding buoys and stop," *IEEE Rob. and Autom. Letters*, vol. 7, no. 3, pp. 8061–8068, Jul. 2022.

[4] O. Tortorici, C. Anthierens, V. Hugel, and H. Barthelemy, "Towards active self-management of umbilical linking rov and usv for safer submarine missions," in *IFAC-PapersOnline*, vol. 52, no. 21. Daejeon, Republic of Korea: Elsevier, 2019, pp. 265–270.

[5] M. Laranjeira, C. Dune, and V. Hugel, "Catenary-based visual servoing for tether shape control between underwater vehicles," *Ocean Engineering*, vol. 200, p. 107018, 2020.

[6] R. G. Duncan, M. E. Froggatt, S. T. Kreger, R. J. Seeley, D. K. Gifford, A. K. Sang, and M. S. Wolfe, "High-accuracy fiber-optic shape sensing," in *Sensor Systems and Networks: Phenomena, Technology, and Applications for NDE and Health Monitoring 2007*, K. J. Peters, Ed., vol. 6530, Int. Society for Optics and Photonics. San Diego, CA, USA: SPIE, 2007, pp. 487 – 497.

[7] I. Floris, J. M. Adam, P. A. Calderón, and S. Sales, "Fiber optic shape sensors: A comprehensive review," *Optics and Lasers in Engineering*, vol. 139, p. 106508, 2021.

[8] S.-C. Yu, J. Yuh, and J. Kim, "Armless underwater manipulation using a small deployable agent vehicle connected by a smart cable," *Ocean Engineering*, vol. 70, no. 23, pp. 149–159, 2013.

[9] C. Xu, K. Wan, J. Chen, C. Yao, D. Yan, and C. Wang, "Underwater cable shape detection using shapetape," in *Oceans*. MTS/IEEE, 2016, pp. 1–4.

[10] J. Frank, R. Geiger, D. R. Kraige, and A. Murali, "Smart tether system for underwater navigation and cable shape measurement," 2013, uS Patent 8,437,979.

[11] N. O.A. and I. Schjølberg, "Finite element cable-model for remotely operated vehicles (rovs) by application of beam theory," *Ocean Engineering*, vol. 163, pp. 322–336, 2018.

[12] Y. Meng, X. Xu, and M. Zhao, "Dynamics calculation of complex deep-sea cable system based on hybrid optimization algorithm," *Ocean Engineering*, vol. 200, p. 107041, 2020.

[13] S. Soylu, B. Buckham, and R. Podhorodeski, "Dynamics and control of tethered underwater-manipulator systems," in *Oceans*. Seattle, WA, USA: MTS/IEEE, 2010, pp. 1—-8.

[14] S. Hong, K. Ha, and J. Kim, "Dynamics modeling and motion simulation of usv/uuv with linked underwater cable," *J. of Marine Science and Engineering*, vol. 8, no. 5, 2020.

[15] J. Drupt, C. Dune, A. I. Comport, S. Seillier, and V. Hugel, "Inertial-measurement-based catenary shape estimation of underwater cables for tethered robots," in *IROS (to appear)*. Kyoto, Japan: IEEE/RSJ, 2022.

[16] J. Estevez and M. Graña, "Robust control tuning by pso of aerial robots hose transportation," in *Bioinspired Computation in Artificial Systems*, J. M. Ferrández Vicente, J. R. Álvarez-Sánchez, F. de la Paz López, F. J. Toledo-Moreo, and H. Adeli, Eds. Springer International Publishing, 2015, pp. 291–300.

[17] K. A. Talke, M. De Oliveira, and T. Bewley, "Catenary tether shape analysis for a uav - usv team," in *IROS*. Madrid, Spain: IEEE/RSJ, 2018, pp. 7803–7809.

[18] D. S. D'Antonio, G. A. Cardona, and D. Saldaña, "The catenary robot: Design and control of a cable propelled by two quadrotors," *IEEE Rob. and Autom. Letters*, vol. 6, no. 2, pp. 3857–3863, 2021.

[19] M. Laranjeira, "Visual servoing on deformable objects: An application to tether shape control," Ph.D. dissertation, University of Toulon, Toulon, France, 2019.

[20] J. C. Lagarias, J. A. Reeds, M. H. Wright, and P. E. Wright, "Convergence properties of the nelder–mead simplex method in low dimensions," *SIAM Journal on Optimization*, vol. 9, no. 1, pp. 112–147, Jan. 1998.